

Extinction and Sky Brightness at Two Solar Observatories

M.J. Penn¹, H. Lin², A.M. Schmidt³, J. Gerke⁴ and F. Hill¹

¹*National Solar Observatory * , 950 N Cherry Av, Tucson AZ 85719*

²*Institute for Astronomy, University of Hawaii, 2680 Woodlawn Drive, Honolulu, HI 96822-1897*

³*Cornell University, Department of Physics, 109 Clark Hall, Ithaca, NY 14853-2501*

⁴*University of Arizona, Department of Astronomy, Steward Observatory, 933 N Cherry Av, Tucson AZ 85721-0065*

Abstract. The Advanced Technology Solar Telescope site survey Sky Brightness Monitor simultaneously images the solar disk and the sky to about 8 solar radii in four wavelengths at 450, 530, 890 and 940nm. One day of data from Mees Solar Observatory on Haleakala and from the National Solar Observatory at Sacramento Peak (Sunspot, New Mexico) are analyzed. Both sites show strong Rayleigh extinction, but while Haleakala shows a larger aerosol component, Sunspot shows a large variation in the aerosol component. Overall the Haleakala extinction varies as λ^{-2} whereas the Sunspot extinction changes from about $\lambda^{-3.5}$ to about λ^{-2} , suggesting an increasing aerosol component during the day. Water vapor absorption measurements from both sites are similar, though Sunspot shows larger time variations than Haleakala. The instrument corrected sky brightness from both sites show comparable values, and again the Sunspot data show more variations. The sky brightness values show a radial dependence of sky brightness of $r^{-0.1}$ at Haleakala, but a dependence of $r^{-1.0}$ at Sunspot. The wavelength variation of the sky brightness at Haleakala is relatively constant at $\lambda^{-1.5}$ but varies at Sunspot from $\lambda^{-1.5}$ to $\lambda^{-0.1}$ again suggesting an increasing aerosol contribution during the day at Sunspot. Finally dust measurements near the ground are compared with the extinction wavelength exponent for data taken at Haleakala on 24 Feb 2003. The measurements suggest more large dust particles are present near the ground than averaged over the whole air column.

1. Introduction

The Advanced Technology Solar Telescope (ATST) is a 4m off-axis all-reflecting telescope being planned by the National Solar Observatory (NSO). The ATST will be used for high-resolution solar disk observations, as well as off-limb observations of the solar corona at

* Operated by the Association of Universities for Research in Astronomy, Inc. (AURA), under cooperative agreement with the National Science Foundation



near-infrared wavelengths. Scattering from mirror roughness should be minimal, and procedures for minimizing dust accumulation on the ATST primary mirror are being studied. In addition to these instrumental parameters, the location of the ATST will also influence the ability of the telescope to observe the solar corona. The primary goal with the ATST Sky Brightness Monitor (SBM) data is to produce calibrated sky brightness measurements at the six ATST test sites. While atmospheric tests at many sites have been done by a variety of authors, few tests probe the near-Sun region of the sky which is critical for solar coronal observations. In order to relate these new measurements to historic observations, primarily at NSO Sac Peak and UH/IfA Haleakala, the SBM has a wavelength channel at 530nm, near the coronal Fe XIV green-line. Calibration of the SBMs with the visual sky brightness Evans's photometers (Evans 1948) is also facilitated at this wavelength. Six SBM instruments were deployed to the ATST test sites and began observations in May 2003. Calibrated sky brightness, solar intensity extinction, and absorption in a water vapor band at 940nm are measured in order to better understand the atmospheric properties at each of the sites.

2. Data and Analysis

Data from Haleakala and Sunspot are used in this initial data analysis. The Haleakala data are comprised of 95 images from 08 May 2003 from 16:08 to 23:58 UT covering a range in airmass of about 15.5 (morning) to 1.09 (afternoon). The Sunspot data are comprised of 70 images from 16 May 2003 from 15:39 to 21:24 UT covering a range in airmass of about 1.45 (morning) to 1.22 (afternoon). The Haleakala observations started shortly after sunrise, whereas the Sunspot data were collected around local noon. These two days were selected from observations during May through July of 2003 for their many hours of continuous data, relatively stable atmospheric extinction, and because the sky brightness at both sites was comparable. The sites themselves have a similar altitude, but the local environment is very different; the Haleakala site is located on a dormant Hawaiian volcano in the middle of the Pacific ocean, whereas Sunspot is located in a high altitude forest in the desert region of south-central New Mexico.

The SBM instruments are thoroughly described elsewhere (Lin and Penn, 2003). The image consists of a 320×240 pixel region with 42 arcsecond pixels. The entire field of view is seen through four filters with central wavelengths at 450, 530, 890 and 940nm and widths of about 10nm each. The solar disk is additionally filtered by a neutral

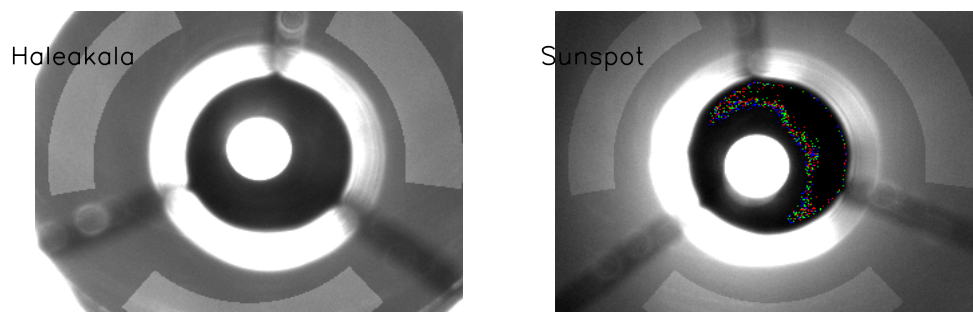


Figure 1. Sample ATST SBM images from Haleakala and Sunspot at 890nm. The central region shows the solar disk filtered by the neutral density occulter; the shadows for the three occulter support arms can be seen at roughly 120-degree intervals. Outside of this occulter region are bright diffraction rings from the occulter edges. In the Haleakala image diffraction from the front of the telescope tube can be seen at the extreme edges of the field of view. The three highlighted arc regions in each image show the field-of-view used to make the sky brightness measurements.

density occulter which has measured transmission at 130, 130, 250 and 250×10^{-6} in the four wavelength channels respectively. The sky beyond the solar disk is not attenuated by this neutral density filter, but passes through the wavelength filter and then to the detector. In this way a simultaneous measurement of the apparent solar disk brightness and the sky brightness is made with one exposure. In the images in Figure 1 sample frames can be seen from both sites taken at 890nm. The central region of each image shows the highly attenuated solar image. The solar disk is not saturated in the image, but the contrast in Figure 1 is stretched to show faint structure in the sky region. Diffraction rings from the neutral density occulter are seen surrounding the central field-of-view. The brightness of the diffracted light ring changes with position angle around the ring due to the spatial position of the solar disk in the image. Three dark gaps in this diffracted light ring can be seen and shadows (and additional reflections) can be seen in the sky field-of-view from the SBM occulter support arms.

The data in this work is processed and analyzed with Interactive Data Language (IDL) from Research Systems Inc. Dark images are automatically subtracted from the SBM images during collection, and flat fielding is not done on these images since the cameras show little pixel to pixel variation (Lin and Penn, 2003). During the day the solar image moves due to tracking problems since the SBM has no guider. In each image the solar disk center is computed by a centroiding technique. Solar disk intensities are computed in two ways: a central solar intensity

is computed within a 5 pixel ($0.10R_{\odot}$) central circular region, and a mean solar intensity is computed using all pixels out to $1R_{\odot}$.

In Figure 1 the highlighted regions in each image shows the areas used to make sky brightness measurements. First a valid sky region is established outside of the diffraction rings and between the occulter support arms in the images. Then based on the computed solar disk center in the image, a section of the sky extending from 4.5 to $7.8R_{\odot}$ is defined. A mean sky brightness is computed within this region for each image as is the the mean distance of all the averaged pixels. In order to investigate sky brightness changes with radial position the sky field-of-view is divided into 11 annuli with widths of $0.3R_{\odot}$ and the mean brightness is computed for each annuli. In some cases solar image motion precludes a meaningful measurement of the brightness in the inner or outer annuli.

For each image the time of the observation is used to compute the solar RA and DEC with a modified version of the IDL program `sun.pro` (from R. Sterner at NASA/GSFC based on Meeus, 1988) and then this position with the site location and elevation are used as inputs into the IDL routine `eq2hor.pro` (from C. O'Dell at University of Wisconsin-Madison, available in the IDL `astrolib` library) to compute the apparent azimuth and elevation angles of the Sun.

3. Extinction Measurements

Figure 2 shows a sample plot of the logarithm of the mean solar intensity versus the air mass for both sites. If the observed solar intensity varies as $I(t) = I_0 e^{-\tau(t)}$ and we define the optical depth $\tau(t) = \kappa M(t)$ where κ is the extinction and M is the air mass, then the logarithm of intensity versus air mass should be a linear plot $\ln(I(t)) = \ln(I_0) - \kappa M(t)$ with the slope giving the extinction. The solar air mass is computed using a circular atmospheric model as described in Lin and Penn (2003).

Examining the data in detail, the morning and evening solar intensities at the same air mass change. This is particularly true at the Sunspot site, where the curves in Figure 2 show two different measured intensities (morning and afternoon) at the same air mass. This suggests a time varying extinction $\kappa(t)$. To account for changing extinction, the instantaneous extinction is calculated in the data analysis. First a linear fit is made to the morning solar intensity (since it is thought that the atmospheric conditions are more stable in the morning) to determine the zero air mass intensity value $\ln(I_0)$. Then for each measurement at time t the instantaneous extinction is computed as $\kappa(t) = (\ln(I(t)) - \ln(I_0))/M(t)$. As discussed by Stock (1969)

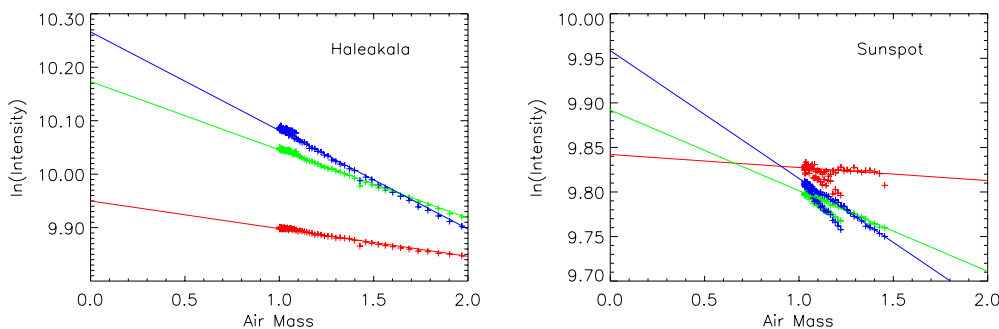


Figure 2. The logarithmic solar disk intensity is plotted versus air mass for data from both sites shown for the 450, 530 and 890nm wavelength channels (blue, green and red plots). The morning observations are fit with a linear function in this plot to obtain the instrumental constant I_0 , and then this constant is used to compute the instantaneous extinction as a function of time for both data sets. The atmospheric extinction in the Haleakala data is seen to be relatively constant since the intensity at a given air mass is single-valued, while the morning and afternoon atmospheric conditions in the Sunspot data show a change.

and recently by Poretti and Zerbi (1993) this technique is valid with stable detectors (this means stable CCD and filters in the case of the SBM) and if the value of I_0 is not changing over time. During one year as Earth's orbital distance from the Sun changes the value of I_0 will fluctuate by 6.5% (this is seen by Andersen et al., 1988) but during one day the changes will not be noticed; also effects from solar brightness oscillations are too small to be noticed.

Figure 3 shows the temporal variation of the extinction at four wavelengths during the day. The extinction in the Sunspot data shows an increase after about 20:30 UT consistent with the intensity variation in Figure 2, while the computed Haleakala extinctions remain relatively constant during the observations. Note that the extinction decreases for longer wavelengths with the exception of the 940nm channel. (The extinction in the 940nm wavelength channel is a combination of extinction and absorption from water vapor, since strong water vapor absorption lines occur in the bandpass of that filter.) The differences between channels are in the range of 0.05 to 0.10.

A decrease of extinction with wavelength is expected if Rayleigh scattering dominates the atmospheric scattering. Rayleigh scattering originates from air molecules or very small particles with radius less than 0.02μ , while aerosol scattering (scattering by haze and dust) is due to larger particles with sizes from roughly 0.3 to 5μ (van de Hulst, 1957). The expected contribution of Rayleigh scattering to the total extinction at each wavelength can be calculated from the atmospheric

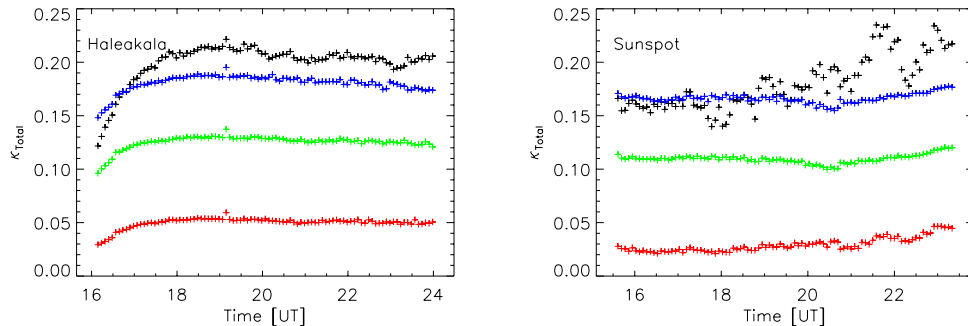


Figure 3. The computed instantaneous extinction $\kappa(t)$ for both sites shown for the 450, 530, 890 and 940nm wavelength channels (blue, green, red and black respectively).

pressure, measured at each site by the ATST weather station. The extinction from Rayleigh scattering $\kappa_R(\lambda)$ can be found from Cox (2000) as $\kappa_R(\lambda) = 8.569 \times 10^{-3} \lambda^{-4} (p/p_0)$ where λ is measured in microns, p is the atmospheric pressure and p_0 is the sea level pressure of 1013.25mbar. The ATST weather stations measured pressures of 716mbar and 722mbar at the Haleakala and Sunspot sites respectively, and the pressure was relatively constant during the day. With the assumption that the total extinction is caused by Rayleigh and aerosol scattering, the aerosol component can be isolated by taking the difference $\kappa_a = \kappa - \kappa_R$. Figure 4 plots this difference as a function of time for both sites. The wavelength differences are now seen to be about 0.01, and the wavelength variation shows more extinction at longer wavelengths. The increase in the aerosol component at Sunspot in all wavelength channels suggests that an increasing level of atmospheric dust may be responsible for the observed increase in the extinction. The negative extinctions seen in the 450nm data from Sunspot suggest that systematic errors in the extinction calculation exist at the level of 0.01. A similar result was found by computing the Rayleigh component using the expression from Martinez Pillet, Ruiz Cobo and Vazquez (1990) $\kappa_R(\lambda) = 1.184 \times 10^{-6} \lambda^{-4.05} (9000 - h)$ where h is the site elevation in meters and wavelength is in microns. However, using this expression there was a larger difference in the aerosol extinction predicted by the three wavelengths than was found using the atmospheric pressure expression. (A better agreement between the extinction at different wavelengths was found if 8300m was used instead of 9000m in the Martinez Pillet, Ruiz Cobo and Vazquez expression.)

Another analysis of the wavelength variation of the extinction follows from a discussion by van de Hulst (1957). The wavelength de-

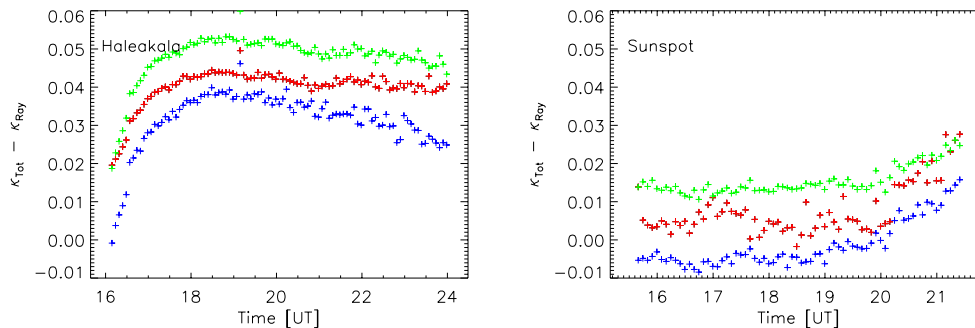


Figure 4. The total extinction minus the Rayleigh scattering contribution computed from the atmospheric pressure measured at each site. The 450, 530 and 890nm SBM wavelength channels are shown as blue, green and red respectively. The total extinction minus the Rayleigh contribution should predict the aerosol extinction. The fact that the predicted aerosol extinction from the different wavelengths is not identical may reveal systematic problems in the extinction calculation, or may be due to a wavelength variation of the aerosol extinction.

pendence of the extinction can be formulated using the power law expression developed by Ångström, $\kappa(\lambda) = C_0 \lambda^{-\alpha}$ where the exponent α is thought to range from 4 for Rayleigh scattering to 0 for neutral scattering by pure aerosols. During a Saharan dust event as seen from the Teide Observatory, Gonzalez Jorge *et al.* (1998) measure a very small value for $\alpha = 0.12$ confirming that during the dust event the atmospheric scattering is neutral. Figure 5 shows a plot of the value of α for both sites as a function of time throughout the day. As discussed by van de Hulst, previous measurements of the extinction exponent have been found to be between 1 and 2; this agrees with the observed values from Haleakala, but the Sunspot values range from 2 to 4, larger than these previous results and suggesting a smaller aerosol component. The time variation of the exponent α is very different at the two sites; the exponent from Haleakala is rather constant, but the exponent from Sunspot varies during the day. The decrease of the exponent from the Sunspot site implies an increasing aerosol component in the atmosphere later in the afternoon, perhaps from wind-blown dust from the nearby White Sands dune fields located west of the observatory.

3.1. WATER VAPOR MEASUREMENTS

The total extinction at 940nm has components due to both scattering and absorption from strong water vapor bands, $\kappa(940) = \kappa_s(940) + \kappa_{water}(940)$ while the observed extinction for the other wavelengths are primarily due to scattering. The scattering extinction at 940nm can be

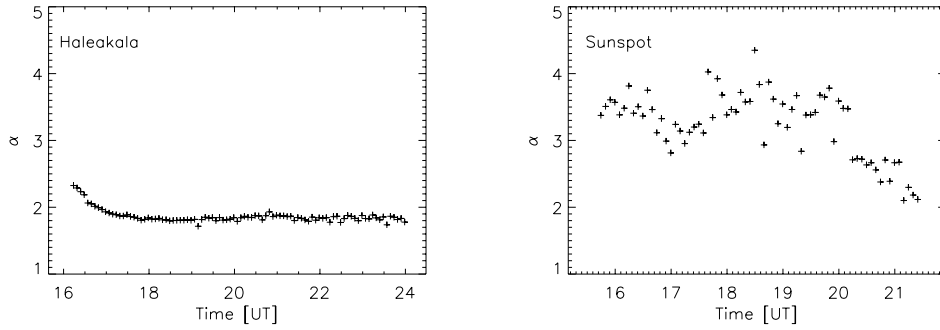


Figure 5. The time variation of the wavelength dependence of the extinction is shown by these plots of α versus time for both sites. The value of α is found by simply fitting a power law to the total extinction at each wavelength. The values measured at Haleakala agree with previous reports, while the values at Sunspot are larger. The decrease in α during the day at Sunspot may reflect an increase in atmospheric aerosols.

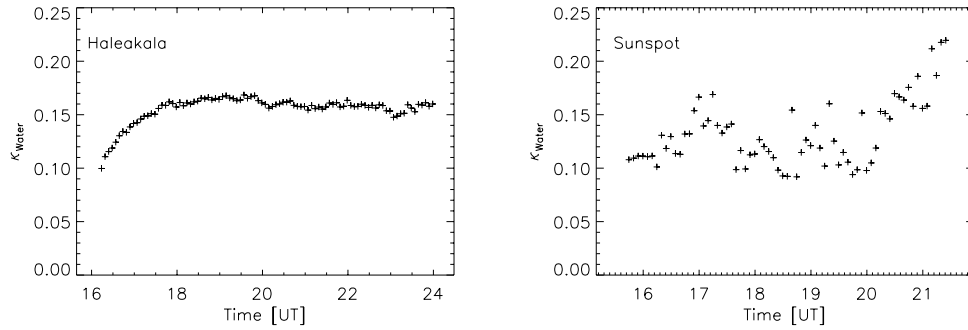


Figure 6. The extinction due to absorption by water vapor spectral lines is shown as a function of time for both sites.

extrapolated from the extinction exponent and the measured extinction at 890nm using the Ångström formula $\kappa_s(940) = \kappa(890)(940/890)^{-\alpha}$, and subtracting this scattering term from the total extinction at 940nm allows the water vapor absorption to be measured. As the extinctions and the wavelength exponent vary with time, the time variation of the water vapor absorption can be found using:

$$\kappa_{water}(940, t) = \kappa(940, t) - \kappa(890, t)(1.056)^{-\alpha(t)}$$

where $1.056 = 940/890$. It is important to note that the instrumental calibration constant is removed by the extinction calculation, and the absorption value computed in this way should be independent of the particular SBM instrument properties.

Figure 6 shows the computed water vapor absorption at 940nm. The value of the absorption is about a factor of five larger than the scattering, showing that water vapor absorption dominates this wavelength channel. While both sites have similar water vapor absorption, the time variation of the water vapor at the Sunspot site is much larger than the relatively constant water vapor absorption seen at Haleakala.

Apart from using the instantaneous extinction values, the columnar water vapor (CWV) content of the atmosphere can be calculated by using the measured solar disk brightness in the 890 and 940nm wavelength channels. Several methods for this analysis are discussed by Schmid et al. (2001). For the SBM data the modified Langley-plot technique discussed by those authors is applicable. Schmid et al. (2001) state:

$$I(\lambda) = \frac{I_0(\lambda)}{d^2} e^{-\kappa M} e^{-a(Mu)^b}$$

where $I(\lambda)$ is the measured intensity, $I_0(\lambda)$ is the instrument calibration constant, d is the Earth-Sun distance in AU, M is the relative air mass, u is the columnar water vapor (or preceptible water), and a and b are constants. With the simplifying assumption that $\kappa(940nm) = \kappa(890nm)$ and then taking the natural logarithm of the ratio of the intensity measured at 890nm to the intensity measured at 940nm the value of u can be found as:

$$u = \frac{1}{M} \left[\frac{1}{a} \ln \left(\frac{I_0(940)I(890)}{I(940)I_0(890)} \right) \right]^{1/b}$$

The instrumental calibration constants at 890 and 940nm are determined with a fit to the zero air mass value of the measured intensity, and then knowing the air mass, intensities and the constants a and b the value of the columnar water vapor can be calculated for each SBM observation.

The values of the constants a and b depend upon the transmission profile of the 940nm filter. These coefficients may be determined using the measured filter profile convolved with a MODTRAN model atmosphere produced with a known CWV value. Unfortunately it was determined that the SBM 940nm filter peak transmission values seem to vary from filter to filter, by as much as 10% and thus the ratio of 890nm to 940nm flux measured by different SBM instruments may be systematically different. This technique will be used after the filter transmissions from each SBM are measured.

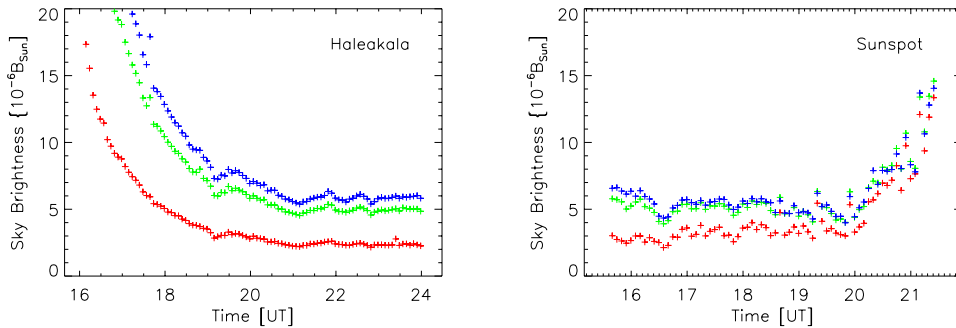


Figure 7. The calibrated sky brightness in the 450, 530 and 890nm wavelength channels (blue, green and red) for the two sites. The instrumental scatter, determined from the zero air mass intercept of the sky brightness, is removed from each plot. The sky brightness is a mean from pixels at 4.5 to $8R_{\odot}$ distances from disk center.

4. Sky Brightness Measurements

The calibrated sky brightness is computed for each image as the mean brightness from 4.5 to 7.8 solar radii divided by the brightness at the center of the solar disk. Martinez Pillet, Ruiz Cobo and Vazquez (1990) show that the calibrated sky brightness varies linearly with the product of the total extinction κ and the air mass M as follows:

$$\frac{I_{sky}}{I_{sun}} = \phi \kappa M + B$$

where ϕ is the atmospheric scattering function which describes the angular distribution of the scattered light and B is the instrumental scatter, which is independent of air mass. Linear fits were made to the measured sky brightness and the optical depth for each site for the 450, 530 and 890nm SBM wavelength channels; however the data did not show a completely linear behavior. There was a variation in the derived instrumental scattering parameters depending on which data points were used, with the Haleakala site showing a range of about $2 \times 10^{-6} I_{sun}$ and the Sunspot site showing a range of about $5 \times 10^{-6} I_{sun}$ in this parameter as the threshold intensity for the sky brightness used in the fit was changed from $200 \times 10^{-6} I_{sun}$ to $12 \times 10^{-6} I_{sun}$. A value of $14 \times 10^{-6} I_{sun}$ was selected as the threshold for fitting the data from both sites. The derived instrumental scatter was found to be 1.5, 1.1 and $2.6 \times 10^{-6} I_{sun}$ for the Haleakala 450, 530 and 890nm wavelength channels. The values for Sunspot were determined to be 2.0, 2.8 and $4.0 \times 10^{-6} I_{sun}$.

In Figure 7 the calibrated sky brightness (in millionths of the disk center intensity) is plotted for both sites for the 450, 530 and 890nm

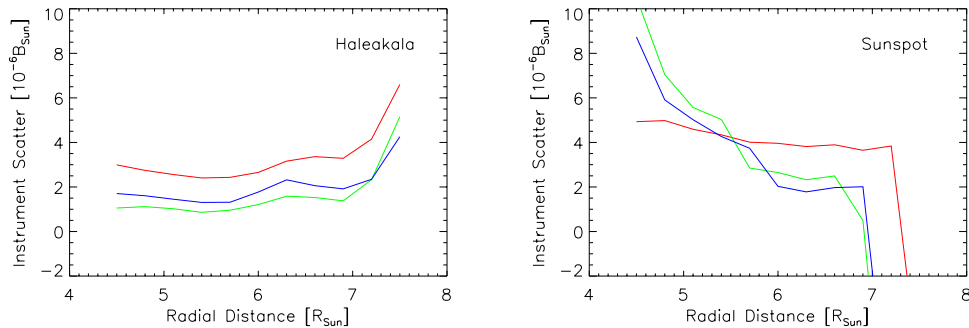


Figure 8. The instrumental scattering function B is computed as a function of radial distance from the center of the solar disk in both the Haleakala and Sunspot SBM instruments at 450, 530 and 890nm (blue, green and red). Note that the Haleakala SBM instrument shows less variation of instrumental scatter than the Sunspot SBM.

wavelength channels of the SBM. The instrumental scattering parameters have been removed from these plots and so the two sites can be directly compared.

The measurement of the sky brightness in different radial bins allows a characterization of the variation of instrumental scattered light B with radial distance from the Sun. Linear fits to the calibrated sky brightness as a function of optical depth were made in each wavelength using data from each radial bin ($0.3R_{\odot}$ in size), and the zero optical depth fit was defined as the instrument scatter and is plotted in Figure 8. The instrumental scatter is relatively constant at Haleakala, but shows larger changes in the Sunspot instrument. At the largest radial distances the 890nm instrumental scattered light is significantly larger than the scatter at 450 or 530nm.

Figure 9 shows the atmospheric scatter parameter ϕ as a function of radial distance in the SBM sky field-of-view for both instruments. Gonzalez Jorge *et al.* (1998) state that Mie scattering produces a strong wavelength dependence in the scattering function, but the normalized plots that they present cannot be directly compared with these computed values. Also as discussed by Gonzalez Jorge *et al.* (1998) the scattering function produced from Mie scattering should drop as a function of radial distance from the Sun. This is seen in the Haleakala data. However as seen in the Sunspot data, the 450 and 530nm values for ϕ seem to increase with radial distance, and the value at 890nm is very large. This strange behavior suggests that Mie scattering is not the dominant mechanism at Sunspot but which scattering mechanism can produce the observed scattering function is not known. It is possible

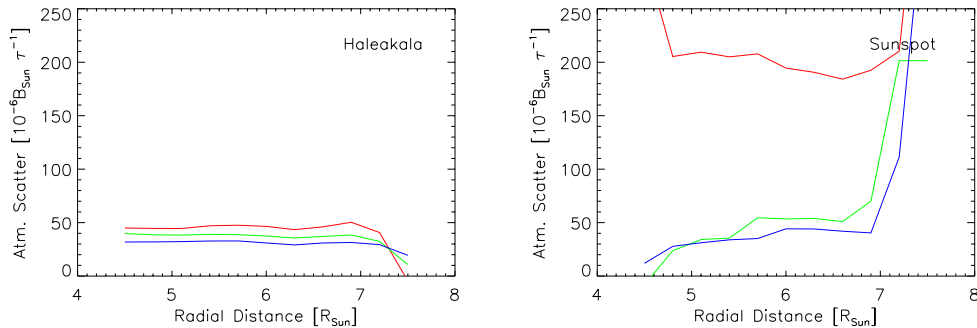


Figure 9. Radial variation of the atmospheric scattering parameter ϕ from each site in 450, 530 and 890nm wavelength channels (blue, green and red). The large variations seen in the Sunspot site strangely suggest an increasing scatter at larger distances.

that scattering off of flying insects or airborne pollen, both of which are common in the forest around Sunspot, may be responsible.

After determining the instrumental scatter in each radial bin, the radial variation of the sky brightness itself can now be determined from each site; here only data from 4.5 to 6.0 solar radii were used. In this analysis, the instrumental stray light computed for each radial bin were subtracted, and then the calibrated brightness was fit with a power law $I_{sky}/I_{sun} = C_1 r^{-\beta}$ where β is the radial exponent. Previous work by Martinez Pillet, Ruiz Cobo and Vazquez (1990) show this exponent to be very close to zero over the range from 1.2 to 1.8 solar radii (see his Figure 2). But measurements presented by Gonzalez Jorge *et al.* (1998) give a range of values with $\beta = 2.5$ to $\beta = 2.8$ at wavelengths from 417 to 785nm from 1.1 to 2 solar radii.

A plot of the radial exponent for the SBM data is shown in Figure 10 for the 450, 530 and 890nm channels as a function of time for both sites. Note that the range of angular distances sampled by the SBM have not been explored by previous work. Although the radial distances sampled by the SBM are larger than the distances in previous work, the values from the Haleakala site are rather close to zero, roughly in agreement with the measurements from Martinez Pillet, Ruiz Cobo and Vazquez (1990). The Sunspot values show a variation during the day, and the increase in the exponents supports the aerosol increase suggested by the extinction data.

The wavelength dependence of the sky brightness can be investigated using the power law expression of Ångström so that $I_{sky}/I_{sun} = C_2 \lambda^{-\gamma}$. This is the same as the wavelength behavior for the atmospheric extinction discussed previously, and makes the assumption that the scattering

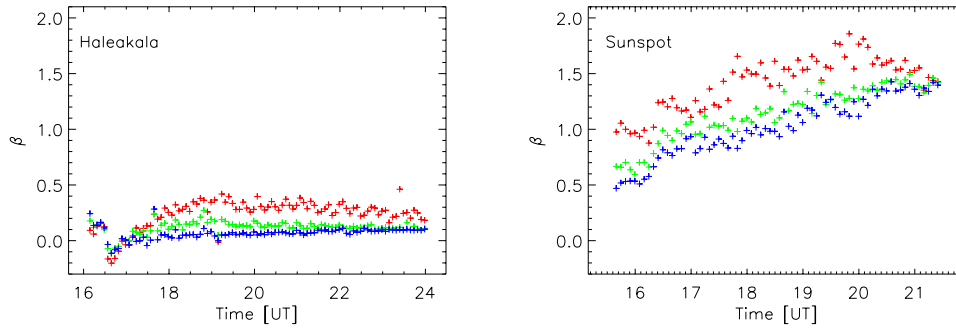


Figure 10. The radial variation of the sky brightness is measured for both sites in the 450, 530 and 890nm channels of the SBM. The Haleakala site shows little variation with radial distance, while the Sunspot site shows a stronger variation.

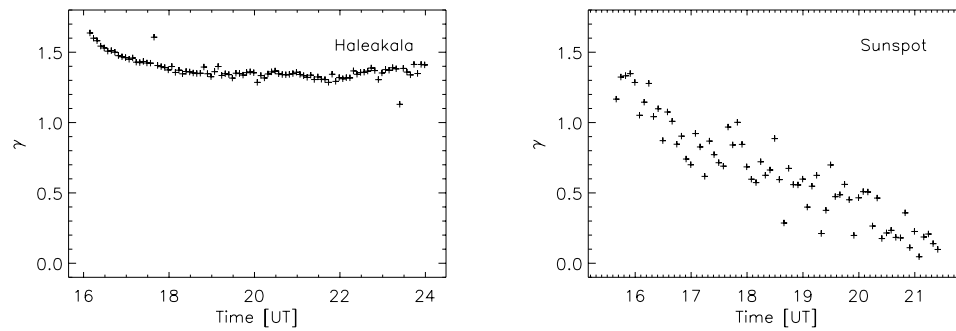


Figure 11. The wavelength exponent γ of the scattered sky brightness is shown as a function of time for both sites. The Haleakala data seems constant and is in agreement with earlier work, but the Sunspot exponent shows a drop during the day, indicating an increase in aerosol scattering.

function ϕ is independent of wavelength. Again the exponent γ is thought to range from 4 for Rayleigh scattering to 0 for neutral scattering by pure aerosols. The mean value of this sky brightness exponent quoted by Gonzalez Jorge *et al.* (1998) was 1.7. The mean sky brightness measurements from the SBM as a function of time were corrected for instrumental scatter and fit with a power law; the value of the exponent γ is shown in Figure 11. The Haleakala exponent is relatively constant and equal to about 1.5, close to the value reported by Gonzalez Jorge *et al.* (1998). The Sunspot exponent starts out at this value, but then falls during the day. This is further evidence that the aerosol scattering at the Sunspot site increased during the day, as a value of $\gamma = 0$ would represent neutral scattering from dust.

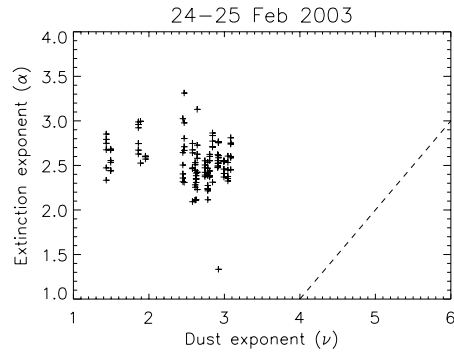


Figure 12. Dust size distribution exponent ν from 24 Feb 2003 at the Haleakala site are compared with the atmospheric extinction wavelength parameter α . The expected relationship is shown by the dashed line. The ground-level dust has many more large particles than seen in the atmospheric column.

5. Dust Measurements

The value of the wavelength extinction exponent α should be related to the exponent in the size distribution ν of the atmospheric particles responsible for the scattering. Using a simple power law for the dust distribution from van de Hulst (1980) where $n(r) = r^{-\nu}$ the expected relationship is $\alpha = \nu - 3$. The dust monitor equipment in the SBM instruments measures the total number of particles with sizes greater than five threshold sizes of 0.3, 0.5, 1.0, 2.0 and 5.0 microns. To obtain number counts we can difference these integrated values and use mean sizes of 0.4, 0.75, 1.5 and 3.5 microns for the resulting bins. A power law is fit to each measurement and a value for the size distribution exponent ν is computed. Since there are five threshold measurements there are four values for which $n(r)$ can be computed at every sample time. A linear fit using all four values results in ν that is lower than if just the two smallest radius sizes are used in the fit.

The size distribution exponents (computed from the smallest bins) from Haleakala on 24 Feb 2003 are shown in Figure 12, along with the atmospheric parameter α computed from the data from that day. The line shows the expected relationship. For a given value of α the measured value of ν is much smaller than expected, which implies that at the ground level of the SBM there are more larger dust particles than in the air column between the SBM and the Sun. Unfortunately changes in ν seem uncorrelated with observed changes in α and so in this data the ground dust properties are not a good predictor of extinction in the air column.

6. Summary

One day of ATST SBM data from Haleakala is and Sunspot are analyzed. The extinction and sky brightness at each site are comparable, but more detailed analysis shows differences between the two sites. While Rayleigh extinction dominates both sites, the aerosol extinction is lower at Sunspot but changes more during the day. The water vapor absorption at both sites has a similar average value, but the Sunspot data fluctuates more. The atmospheric scattering function at Haleakala is consistent with expectations from Mie scattering, but the Sunspot function behaves strangely. The radial and wavelength dependence of the sky scattered light at differs at both sites. Several measurements suggest an increase in the atmospheric aerosol component at Sunspot during this day. The different measurement errors from each instrument cannot account for the larger scatter seen in many of the quantities from the Sunspot data. It is likely that changes in the local forest environment at Sunspot during the day are responsible for the larger time variability seen at this site.

Acknowledgements

MJP thanks Rob Hubbard for comments in the manuscript and Michael Hall for selecting the particular days of data used in this study from the SBM data base. JG participated in this project with funding from the ATST Design and Development grant NSF-XXXXX and AMS participated through an independent research class while an undergraduate student at the University of Arizona.

References

- Andersen, B., Domingo, V., Jimenez, A., Jones, A., Korzennik, S., Palle, P.L., Perez Hernandez, F., Regulo, C., Roca Cortes, T., and Tomas, L.L. : 1988, *Solar Physics* **116** 391
- Evans, J. W., 1948, *JOSA* **38** 1083
- Gonzalez Jorge, H., Martinez Pillet, V., Vazquez, M., Palle, P., McGovern, F. and Raes, F. : 1998, *New Astronomy Reviews* **42** 515
- Lin, H. and Penn, M.J. : 2003, Journal, Volume, Page
- Martinez Pillet, V., Ruiz Cobo, B., Vazquez, M.: 1990, *Solar Physics* **125** 211
- Meeus, J. : 1988, *Astronomical Formulae for Calculators* (Willmann-Bell: Richmond VA USA)
- Poretti, E. and Zerbi, F. : 1993, *Astron. Astrophys.* **268**, 369

- Schmid, B., Michalsky, J.J., Slater, D.W., Barnard, J.C., Halthore, R.N., Liljegren, J.C, Holben, B.N., Eck, T.F., Livingston, J.M., Russell, P.B., Ingold, T. and Slutsker, I. : 2001, *Applied Optics* **40** 1886
- Stock, J. : 1969, *Vistas in Astronomy* **11** 127
- van de Hulst, H.C. : 1957, *Light Scattering by Small Particles* (John Wiley Sons: New York)
- van de Hulst, H.C. : 1980, *Multiple Light Scattering: Tables, Formulas and Applications, Volume 2* (Academic Press: New York)